Available online at www.sciencedirect.com
ScienceDirect
Trans. Nonferrous Met. Soc. China 26(2016) 175−184
Transactions of Nonferrous Metals Society of China
www.tnmsc.cn

# Corrosion and wear behaviors of PVD CrN and CrSiN coatings in seawater

Lei SHAN[1,2,3], Yang-rong ZHANG[1,2], Yong-xin WANG[1,2], Jin-long LI[1,2], Xin JIANG[1,2], Jian-min CHEN[1,2]

1. Key Laboratory of Marine Materials and Related Technologies, Ningbo Institute of Materials Technology and Engineering, Chinese Academy of Sciences, Ningbo 315201, China;
2. Zhejiang Key Laboratory of Marine Materials and Protective Technologies, Ningbo Institute of Materials Technology and Engineering, Chinese Academy of Sciences, Ningbo 315201, China;
3. Department of Mechanical, Zhejiang Textile and Fashion College, Ningbo 315211, China

Received 12 January 2015; accepted 31 October 2015

**Abstract:** To improve the tribological performance of 316L in seawater, the CrN and CrSiN coatings were deposited by multi-arc ion plating. The coatings were systematically characterized. Corrosion properties were evaluated by immersion test and anodic polarization measurement. The friction and wear properties of the CrN and CrSiN coatings were investigated by ball-on-disk tribometer in artificial seawater. The results show that the CrN coating has strong (111) and (200) preferred orientations and the intensity of the peaks decreases for the CrSiN coating. The hardness of the CrSiN coating is higher than that of the CrN coating. The CrSiN coating presents better corrosion resistance in seawater. The friction coefficient and wear rate of the CrSiN coating are lower than those of the CrN coating, indicating positive effect of Si addition on tribological performance in seawater. The coatings could significantly improve the wear resistance of the 316L in seawater.
**Key words:** CrSiN coating; wear; corrosion; seawater

## 1 Introduction

As the exhaustion of land resources, sea resources are going to play important roles in dealing with resource crisis and guaranteeing sustainable development of human society. The sea resource exploitation needs advanced marine equipment. However, the key friction components of marine equipment, such as pumps, open hydraulic drive system, valve, gear, shaft and propeller, have to be operated in seawater during running of the machine [1]. In this case, liquid lubricants do not provide full lubricating effect due to the leakage of oil and the low viscosity of seawater. These components are required to have great wear and corrosion resistance in seawater in order to extend service life and reduce the cost of maintenance of parts. Thus, it is imperative to improve the tribological performance as well as corrosion resistance of marine frictional components. One of the most effective approaches is to take advantage of advanced coatings with good lubrication and protection effects in seawater [2].

PVD (physical vapor deposition) CrN coatings have wide industrial applications as protective material due to the high hardness, good wear resistance and anti-corrosive properties in recent years [3−8]. For instance, the CrN coating can improve erosion-corrosion resistance in slurries [9] and anti-corrosion properties of AISI 304 in 3.5% NaCl (mass fraction) electrolytic solution [10]. Moreover, the CrN coatings have been deposited on 2024 Al alloy to enhance the tribological performance in water [11]. The Si addition to CrN with proper content can enhance hardness and density of the coating, and therefore improve the wear resistance both in air and water [12−14]. As suggested by KIM et al [15], the CrSiN coating deposited on the AISI 4340 cylinder barrel improves friction behavior under tap water up to 1600 r/min without delamination or surface cracking of the coating. The CrSiN coating can decrease corrosion current density and porosity, indicating the contribution of the added Si to the improvement of the corrosion resistance of CrN/stainless steel system in 3.5% NaCl solution [16].

However, the systematical investigations of the

**Foundation item:** Project (51475449) supported by the National Natural Science Foundation of China; Project (LY14E010005) supported by the Zhejiang Provincial Natural Science Foundation of China; Project (Y201534852) supported by the Zhejiang Education Bureau Science Foundation, China; Project (201601HJ-B01034) supported by the Ningbo Municipal Natural Science Foundation, China
**Corresponding author:** Yong-xin WANG; Tel: +86-574-86685175; E-mail: yxwang@nimte.ac.cn
DOI: 10.1016/S1003-6326(16)64104-3

corrosion and wear behaviors for the PVD coating were still limited. The aim of this work is to improve corrosion and wear resistance by the CrN and CrSiN coatings in seawater. Comparative experiments of the corrosion and wear behaviors were carried out in artificial seawater for PVD CrN and CrSiN coatings. The effects of Si addition on corrosion and wear behavior were discussed.

## 2 Experimental

### 2.1 Coating deposition

As the substrates, the 316L stainless steel samples (30 mm × 20 mm × 2 mm) were polished to a surface roughness ($R_a$) below 50 nm and ultrasonically cleaned in acetone and ethanol, respectively. The samples were mounted on a sample holder at 10 cm in front of the targets. The deposition was carried out on a multi-arc ion plating system (Hauzer Flexicoat 850). Prior to deposition, the chamber was pumped down to a base pressure below $4\times10^{-3}$ Pa, then temperature was increased to 400 °C. Thereafter, the substrates were etched by argon bombardments for 2 min with substrate bias voltages of −900, −1100 and −1200 V, respectively, to remove thin oxide layer and other adherent impurities on the substrates. During deposition, the coatings were deposited in $N_2$ (99.95%) atmosphere with a substrate table rotation speed of 3 r/min. The nitrogen pressure was fixed at 4 Pa during the deposition. The Cr and CrSi targets with purity of 99.5% were applied for the deposition of the CrN and CrSiN coatings, respectively. The Si/(Cr+Si) mole ratio of CrSi targets was 2.5%. The depositions were conducted at a bias voltage of −40 V and a target current of 80 A for 4 h for all coatings.

### 2.2 Characterization

The phase structure of the as-deposited coating was investigated by X-ray diffraction (Bruker D8 X-ray facility) using Cu $K_\alpha$ radiation ($\lambda$=0.1541 nm), which was operated at 40 kV and 40 mA. The scanned $2\theta$ angle ranged from 20° to 90° at a scanning speed of 4 (°)/min with a step size of 0.02°. The surface morphologies and cross-sectional images of the coatings were observed by field emission scanning electron microscope (FE-SEM) (FEI Quanta FEG 250) equipped with EDS (OXFORD X-Max). The elemental compositions were determined according to XPS peak area ratios. XPS spectra were obtained by an X-ray photoelectron spectroscopy (AXIS-ULTRA, Kratos) using an Al $K_\alpha$ X-ray source; the source was operated at 12 kV and 10 mA. The survey spectra were collected from 0 to 1200 eV with pass energy of 160 eV. High resolution scans for the elements were performed with pass energy of 20 eV.

The coating adhesion was measured by scratch tester (CSM Revetest) with a conical diamond tip of 0.2 mm radius and 120° taper angle. The measurements parameters were as follows: the table speed of 6 mm/min, loading rate of 118 N/min, loading scale of 0−100 N and scratch length of 3 mm. The acoustic emission was detected when the film was broken and the load at the point of breaking was called the adhesive critical load (LC). Nanoindentation test was carried out using a MTS Nano Indenter@G200 system fitted with a Berkovich indenter using the continuous stiffness measurement (CSM) mode. The maximum indentation depth was 1500 nm. Ten indentations in each sample configured on different areas were performed to have reliable statistics.

Corrosion properties of the coatings were evaluated using two corrosion tests: immersion tests and anodic polarization measurements. The immersion tests were conducted in the artificial seawater at (20±5) °C for 720 h. The artificial seawater was prepared according to Standard ASTM D 1141−98. The chemical composition of artificial seawater is listed in Table 1. In the immersion test, the samples were sealed and an area of 1 $cm^2$ for coating surface was open to directly contact with the test solution. This was to insure that the substrate base metal had no direct contact with the artificial seawater and to confirm corrosion behavior of the coatings under such environment. The polarization measurements were measured by Modulab, Solartron Analytical in seawater. A standard saturated calomel electrode (SCE) was used as a reference electrode and platinum was used as a counter or auxiliary electrode in the test. The contact area was 1 $cm^2$ and the tests were carried out at ambient temperature of (20±5) °C. The electrode potential was raised from −0.9 to 0.5 V at a scanning rate of 2 mV/s.

**Table 1** Chemical composition of artificial seawater (g/L)

| NaCl | $Na_2SO_4$ | $MgCl_2$ | $CaCl_2$ | $SrCl_2$ |
|---|---|---|---|---|
| 24.53 | 4.09 | 5.20 | 1.16 | 0.025 |
| KCl | $NaHCO_3$ | KBr | $H_3BO_3$ | NaF |
| 0.695 | 0.201 | 0.101 | 0.027 | 0.003 |

### 2.3 Tribological test

Wear tests were performed by a reciprocating ball-on-disk tribometer (UMT-3MT tribometer), in sliding contact with WC balls at a room temperature of (20±5) °C. The WC balls were used as the counterparts with a diameter of 3 mm. The tests were conducted in the artificial seawater. A stroke frequency of 5 Hz, constant normal load of 5 N and sliding stroke of 5 mm were used in the experiments and the friction coefficient was continuously recorded during testing. Based on the wear track depth profile detected by Alpha-Step IQ profilometer, the coating wear losses could be obtained after the sliding tests. Then according to the classical

wear equation, the wear rate $W$ could be calculated by the following equation:

$$W=V/(SL) \quad (1)$$

where $V$ is the volume of wear loss, $S$ is the sliding distance and $L$ is the normal load applied.

## 3 Results and discussion

### 3.1 Phase and microstructure

Figure 1 shows the surface morphology and cross-section morphology of the coatings. As seen from Figs. 1(a) and (b), there are many white particles and dimples on the surfaces of the CrN and CrSiN coatings. These small size macroparticles, distributing dispersedly in the coating, have an irregular shape and protrude out of the coating surface. The size of macroparticles for the CrSiN coating is slightly smaller than that for CrN. The EDS analysis indicates that the CrN coating mainly contains Cr and N elements, while the CrSiN coating mainly contains Cr, Si and N elements. As seen from Fig. 1(c), a distinct columnar structure with particles throughout the coating in depth direction is observed for the CrN coating. However, the columnar feature and grain size are reduced via Si addition (Fig. 1(d)), which may be attributed to the formation of $SiN_x$ layer at the grain boundaries and the interrupt of the columnar crystal growth [17,18]. Since cracks may exist at interfaces of particles or columnar crystals, distinct columnar structure indicates a loose coating structure, while few columnar crystals suggest a dense structure. Therefore, it can be considered that the CrSiN coating presents a denser structure than the CrN coating.

To further confirm the composition and element chemical state of the CrSiN coatings, the XPS spectra of Cr $2p_{3/2}$, N 1s, O 1s and Si 2p were investigated, as shown in Fig. 2. As seen from Fig. 2(a), the deconvoluted Cr $2p_{3/2}$ peak is composed of two chemical states, namely CrN (574.5 eV) [19] and $Cr_2O_3$ (576.7 eV) [20]. This indicates that some Cr are bonded to oxygen in the surface region, which may be attributed to the oxygen contamination occurred before the test and during the deposition. In Fig. 2(b), the N 1s peak at 396.8 eV can be attributed to CrN [21] while the peak related to 397.9 eV can be identified as $Si_3N_4$ bond [22], which agrees well with the published values [23]. In Fig. 2(c), the O 1s peak indicates the main component can exist as $Cr_2O_3$ (530.9 eV). As seen from Fig. 2(d), the Si 2p spectrum shows a component (101.8 eV) which can be assigned to the $Si_3N_4$. However, the relatively weak peak indicates a low content of Si—N bond.

Figure 3 shows the X-ray diffraction patterns of the CrN and CrSiN coatings. It is clear that the coatings have strong (111) and (200) preferred orientations. The peaks corresponding to the CrN(220) and CrN(311) are also observed [24,25]. Furthermore, the weakening and broadening peaks of the (111) and (200) planes are observed for CrSiN coating, indicating a fine crystalline structure for the coating. The diffraction peaks for CrSiN shift to lower angles compared with the CrN coating,

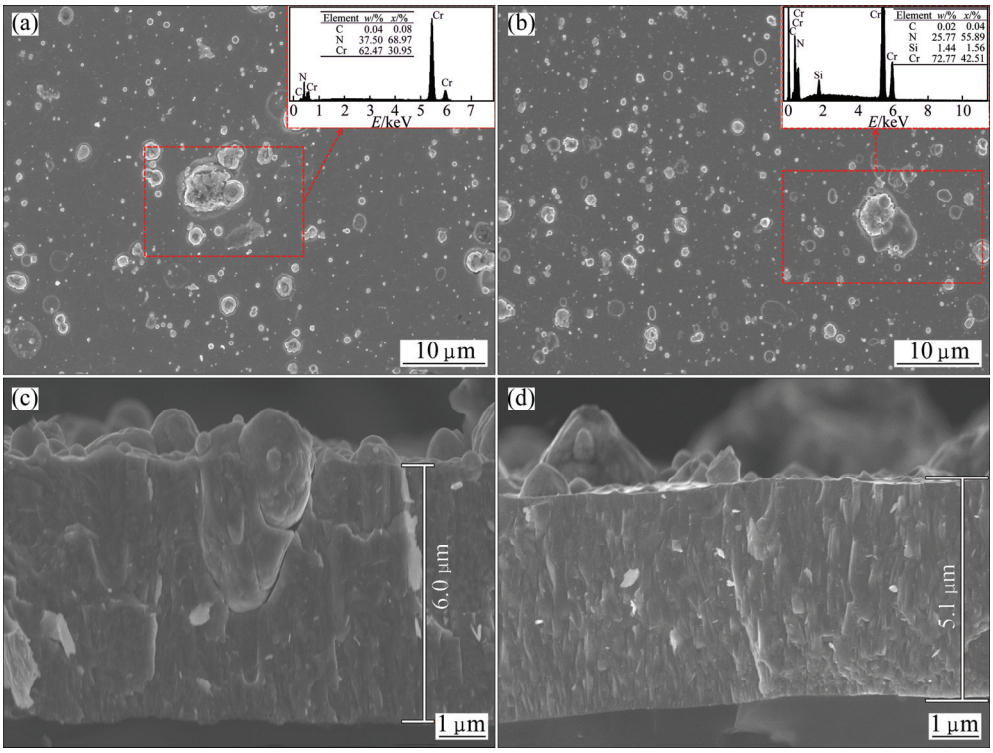


**Fig. 1** Surface and cross-section morphologies of CrN and CrSiN coatings: (a) Topograph of CrN coating; (b) Topograph of CrSiN coating; (c) Cross-section image of CrN coating; (d) Cross-section image of CrSiN coating

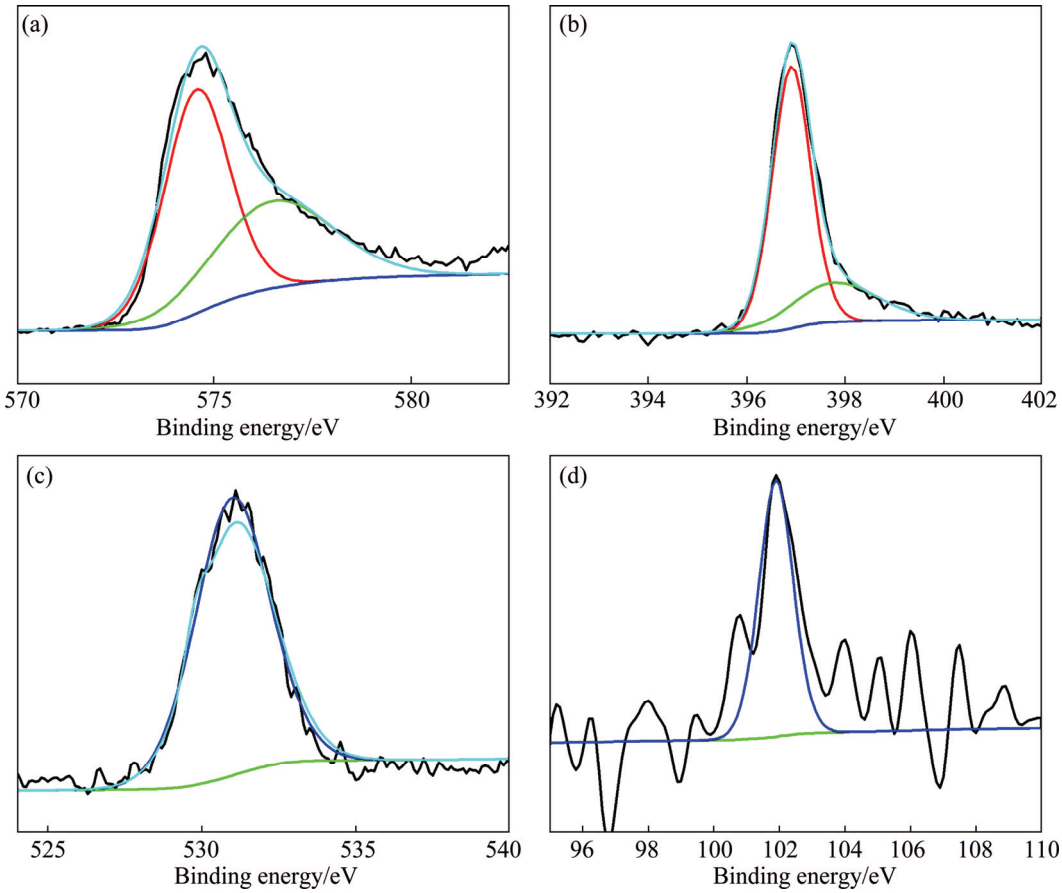


**Fig. 2** XPS spectra of CrSiN coating: (a) Cr 2p $_{3/2}$; (b) N 1s; (c) O 1s; (d) Si 2p

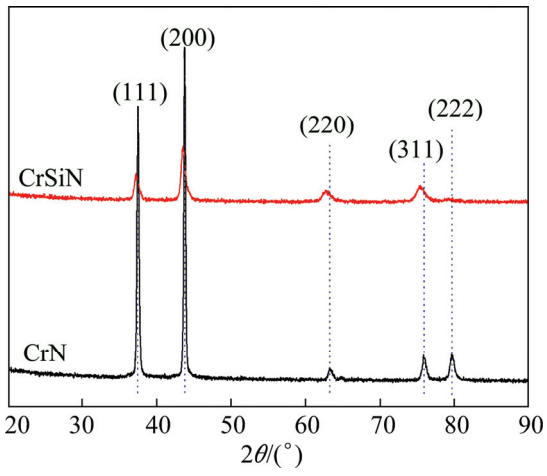


**Fig. 3** XRD patterns of CrN and CrSiN coatings

which may be attributed to the Si atoms dissolved into CrN lattice. Such behavior is generally observed in the case when the added element (Si) is soluble in the polycrystalline network (CrN) to form a solid solution [26].

### 3.2 Mechanical properties

Figure 4 shows a typical acoustic emission−load graph and track morphology of CrN and CrSiN coatings. The critical load (LC) is determined as load corresponding to a sudden increase of acoustic emission signals which represents coating delamination. The LC1 represents crack initial load during scratching. In Fig. 4(a), the curve of acoustic emission is smooth and steady when the normal load is less than 20 N. When the load increases to about 25 N, severe fluctuation of the acoustic signal occurs, indicating that the intensive crack and delamination of the coating take place. The LC1 for the CrN coating is about (25±4) N. However, the acoustic signal for the CrSiN coating is steady below the normal load of 37 N. The LC1 for the CrSiN coating is (37±3) N. The adhesion of the coatings is increased by addition of Si element due to the solid solution strengthening and the grain refining strengthening. When the load increases further to 48.5 N, intensive cracks take place, resulting in broken coating fractions inside track and some delamination in the scratch track.

Figure 5 shows the hardness of the coatings with a maximum indentation depth of 1500 nm. Significant contribution to the hardness from substrate is observed with the increase of indentation depth. According to the continuous stiffness measurement (CSM) mode, the hardness value can be obtained from the platform of the curve (depth between 200 and 400 nm). The hardness of

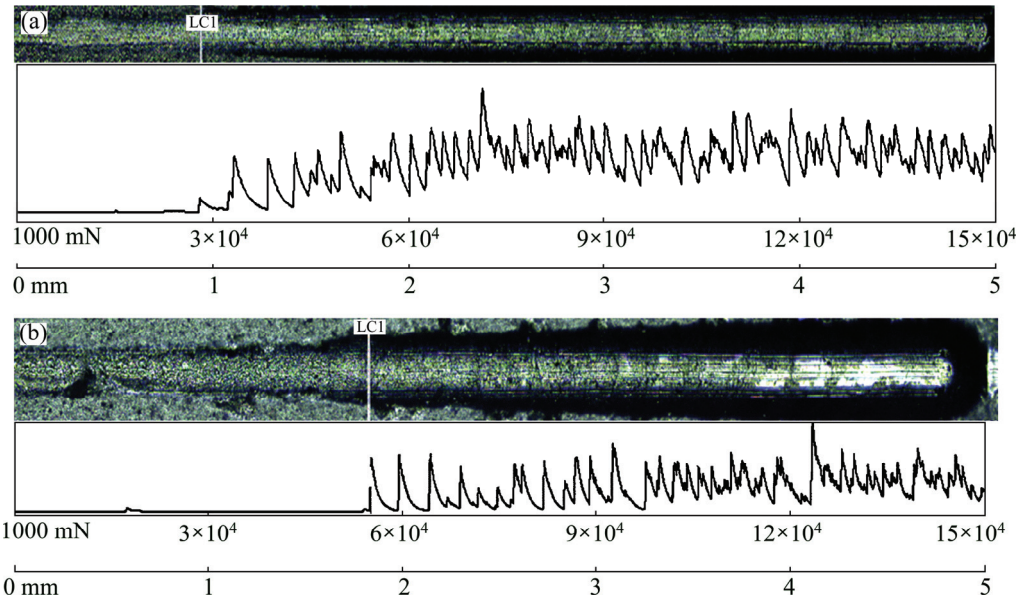


**Fig. 4** Indenter track and scratch test results of CrN coating (a) and CrSiN coating (b)

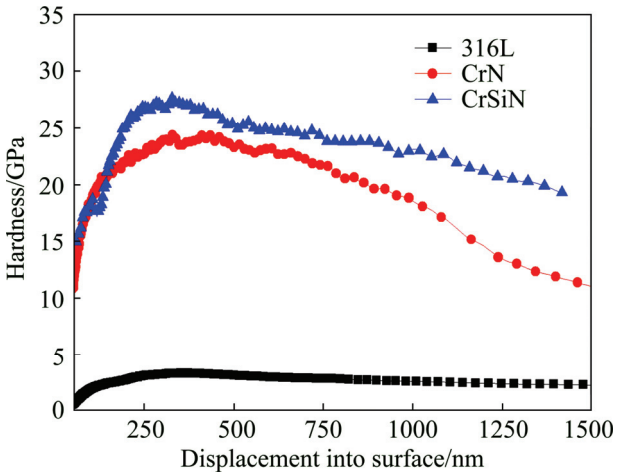


**Fig. 5** Variation of hardness with indentation depth of coatings and 316L

the CrSiN coating ((27±3) GPa) is higher than that of the CrN coating ((24±2) GPa), which may be attributed to the solid solution hardening and the refining strengthening. Compared with the hardness of the substrate (about 3 GPa), both coatings present much higher hardness.

### 3.3 Corrosion properties

Immersion test results of the coatings are shown in Fig. 6. The surface morphology of the coatings after immersion test has no penetrated pinholes or pitting corrosion (Figs. 6(a) and (b)), indicating good corrosion resistance of the coatings in seawater. It may be due to removing the macroparticles of the coating surface, which may fill the cracks and pinholes in the coatings during the test. This is possible to reduce or block coating defects propagation, which prevents the local corrosion at the substrate/coating interface. Compared with the coatings before the immersion test (Figs. 6(c) and (d)), there is no large difference between them which confirms the excellence corrosion resistance of the coatings.

In order to evaluate the anodic dissolution of the coatings, the polarization tests were investigated in seawater. As shown in Fig. 7, it is clear that the coatings have lower anodic current densities compared with 316L substrate. Because it is known that CrN coatings are chemically inert in $Cl^-$ solution. Therefore, the coatings can separate the substrate from the aggressive environment and therefore protect the substrate if the coatings were free of defects such as cracks and pinholes. However, the formation of those defects in ceramic coatings, in reality, is almost impossible to avoid totally. Thus, the CrN coating slightly improves the corrosion resistance of 316L in seawater. It was observed that the anodic current density value of CrSiN is lower than that of CrN, which can be attributed to the denser structure and less cracks and pinholes of the coating. Since micro-defects may exist at interfaces of particles or columnar features, coarse particles and distinct columnar feature indicate a loose coating structure. Thus, it can be considered that the CrSiN coating with denser structure presents better corrosion resistance than the CrN coating in seawater. The passive-like behavior is observed for the CrSiN coatings. The passive layer mainly contains Cr, N, Si and O elements and filled the cracks and pinholes during the tests, and therefore improves the corrosion response. Moreover, the corrosion potential of the CrSiN coating is the most noble, about −150 mV (vs SCE).

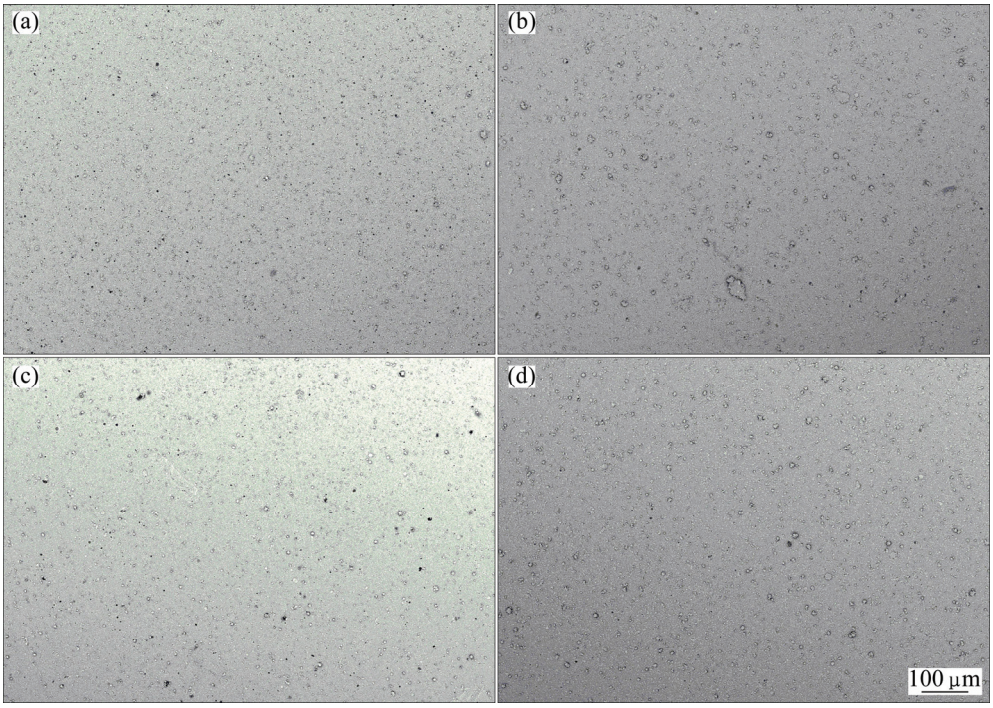


**Fig. 6** Surface images of CrN and CrSiN coatings: (a) CrN coating after immersion tests; (b) CrSiN coating after immersion tests; (c) CrN coating before immersion tests; (d) CrSiN coating before immersion tests

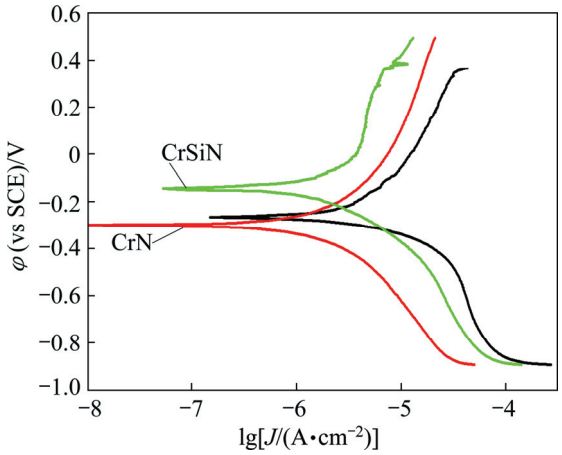


**Fig. 7** Polarization curves of coatings and uncoated 316L

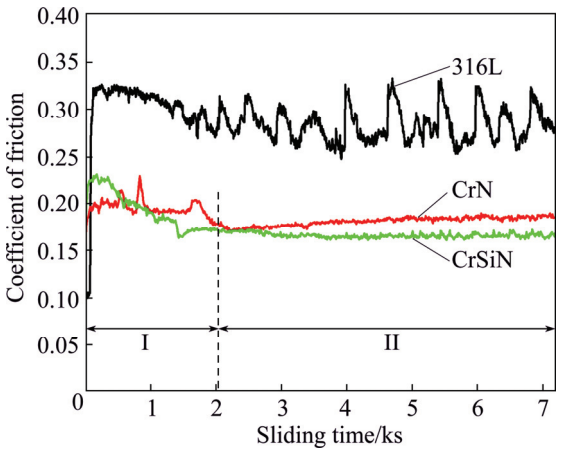


**Fig. 8** Friction behavior of CrN coating and substrate sliding against WC balls in artificial seawater

### 3.4 Friction properties

Figure 8 shows the friction behaviors of the coatings and uncoated 316L sliding against WC balls in seawater, illustrating an excellent lubricating effect of the as-deposited coatings. The friction coefficient of 316L stainless steel sliding against WC balls fluctuates around 0.3 in seawater, but it can be reduced to around 0.17 by the coatings. The friction coefficients for the coatings present relatively high value at first stage (stage I), then reach the relatively steady-state wear stage (stage II). The stage I represents run-in period with relatively high value, which can be attributed to solid−solid contact between tribo-pairs. The solid−solid contact can be easily formed if the sliding interface is unsmooth. The lower value in stage II arises from rapid wear of ball and coating, which causes the interface between tribo-pairs to become smoother and reduce the solid−solid contact region, and increases hydrodynamic lubrication provided by the water condensation from the ambient [27]. Moreover, the wear debrises between the tribo-pair may act as rolling ball to decrease the friction coefficient. Thus, the friction coefficient decreases in seawater after the run-in period. However, the friction coefficient of the CrN coating shows slight ascending trend at stage II. The friction coefficient for the CrN coating in stage II (about 0.186) is higher than that of CrSiN (about 0.165), which can be attributed to the tribochemical reaction in

seawater [28], as follows:

$$Si_3N_4+12H_2O=3Si(OH)_4+4NH_3 \quad (1)$$

$$SiO_2+2H_2O=Si(OH)_4 \quad (2)$$

The formed amorphous hydrate $Si(OH)_4$ dissolved in water, resulting in a thin hydrodynamic lubrication film between the interface, therefore reducing the friction coefficient [11].

### 3.5 Wear properties

Figure 9 shows the cross-sectional profiles of the wear track on the coatings and 316L in seawater. The depth of wear track for 316L is much higher than those for the coatings, which can be attributed to the higher friction coefficient and lower hardness of 316L. The maximum wear depth for the CrN coating is about 0.87 μm, which is higher than that of the CrSiN coating (about 0.45 μm). It may arise from the tribo-corrosion reaction in seawater. Although the immersions test results show that both the CrN and CrSiN coatings present good corrosion resistance in seawater, this is impossible if sliding occurred on the coatings. The passivation layer (mainly contain $Cr_2O_3$) is not easily formed during sliding and the corrosive seawater has a destructive effect on the passivation layer, which protects the clean surface from the corrosive medium. The corrosive medium activates the coating and causes anodic dissolution during sliding, resulting in increased wear loss. The increased wear loss induces more cracks and accelerates the corrosion speed. Finally, synergism effect between corrosion and wear leads to deeper wear track depth for the CrN coating in seawater. Since cracks may exist at interfaces of columnar crystals, distinct columnar crystal indicates a loose coating structure, while few columnar crystals suggest a dense coating. As a result, the seawater penetrates into the cracks of the CrN coating and the synergism effect of corrosion and wear causes the cracks to propagate. Therefore, the relatively dense structure can explain the lower maximum wear depth for the CrSiN coating. Another reason is the higher hardness for CrSiN than that of CrN, because the wear mechanism for the CrSiN coating, as an inert material, is mainly dominated by mechanical wear in seawater [29]. The lower friction coefficient also contributes to the improvement of tribological performance for the CrSiN coating in seawater. As a result, the wear depth for the CrSiN coating is significantly decreased compared with that for the CrN coating.

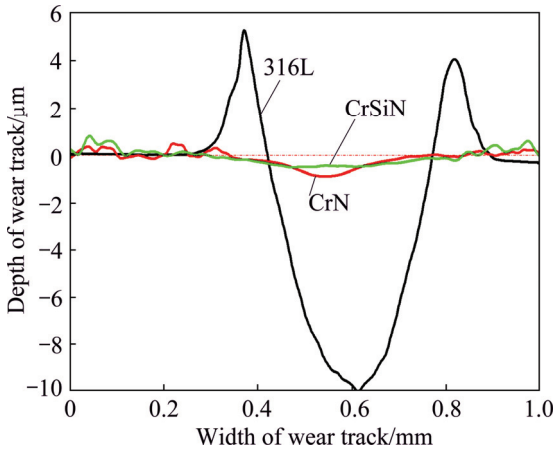


**Fig. 9** Cross profiles of wear track on coatings and 316L

The wear rate of the uncoated 316L is about $6.3\times10^{-6}$ $mm^3/(N\cdot m)$, which is much higher than those of the coatings. The wear rate of the CrSiN coating is about $3.4\times10^{-7}$ $mm^3/(N\cdot m)$, which is lower than that of the CrN coating (about $4.6\times10^{-7}$ $mm^3/(N\cdot m)$). As seen from Fig. 10(a), there are flake pits in the wear track of the CrN coating. However, the flake pits can be eliminated by the addition of Si elements (Fig. 10(b)). The formation of flake pits can be attributed to the propagation of micro-cracks. When the coating slides against WC ball in seawater, the medium can penetrate into the micro-cracks. The coating elements at the crack tip are activated and weakened by $Cl^-$ in seawater during the sliding. This would promote the propagation of the crack. On the other hand, the seawater penetrating into

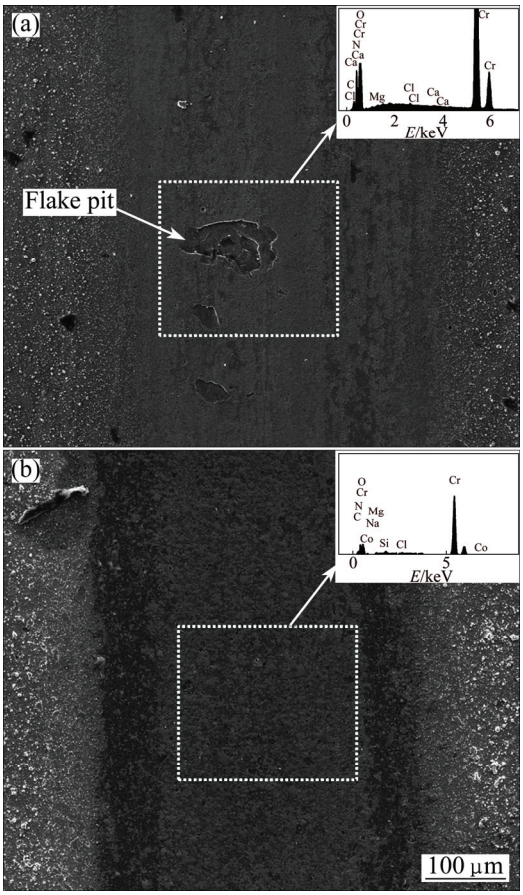


**Fig. 10** SEM images of wear track on coating: (a) CrN coating; (b) CrSiN coating

the cracks induces a wedging action due to its hydrostatic pressure. The wedging action, cooperating with the corrosion effect of the seawater, can cause the subsurface cracks to further propagate and accelerate the formation of flake pits. However, the CrSiN coating with denser structure indicates less crack, which can reduce the formation of flake pits during sliding. As seen from Fig. 10(b), there is a passive layer on the wear track, which may mainly contain $Cr_2O_3$ and $SiO_2$. These particles fill the crack during sliding, preventing the seawater penetrating into the micro-cracks, therefore, inhibiting the wedging action of seawater. As a result, the large flake pits are eliminated by the addition of Si element. The EDS analysis of the wear track for the CrN coating shows that, not only Cr, O and N, but also Mg and Ca elements are on the wear track. This indicates that $Mg(OH)_2$ and $CaCO_3$ might be formed during sliding, which have a good role of lubrication. The EDS analysis of the wear track for the CrSiN coating presents similar results. The Si element is observed, indicating that the $Si(OH)_4$ may be formed during sliding, which could reduce the friction coefficient.

Figure 11 shows the morphologies and the corresponding EDS analysis of the wear scar on the balls. When the CrN coating slides against WC ball in seawater, there are many shallow scratch grooves on the surface of the ball (Fig. 11(a)). Many wear debrises are also observed on the surface of the wear scar. The EDS analysis shows that W, Co, O and Mg elements are on the wear scar, indicating that $Mg(OH)_2$ adheres to the ball surface and oxidation of WC ball occurs during sliding. The morphologies of the wear scar for the CrSiN coating show the similar feature. The wear rates for the balls against CrN and CrSiN coatings are $1.28\times10^{-7}$ $mm^3/(N\cdot m)$ and $1.37\times10^{-7}$ $mm^3/(N\cdot m)$, respectively.

## 4 Conclusions

1) The CrN and CrSiN coatings present good corrosion resistance in seawater and the CrSiN shows the lower anodic current density than CrN coating.

2) The friction coefficients of the coatings are lower than that of 316L in artificial seawater. The friciton coefficient for CrSiN coating is lower than that of CrN coating, which can be attributed to lubricating effect of tribochemical reaction product $Si(OH)_4$ between the interfaces.

3) The wear rates of the coatings are much lower than that of 316L in artificial seawater. The CrSiN coating presents the lowest value due to the lower

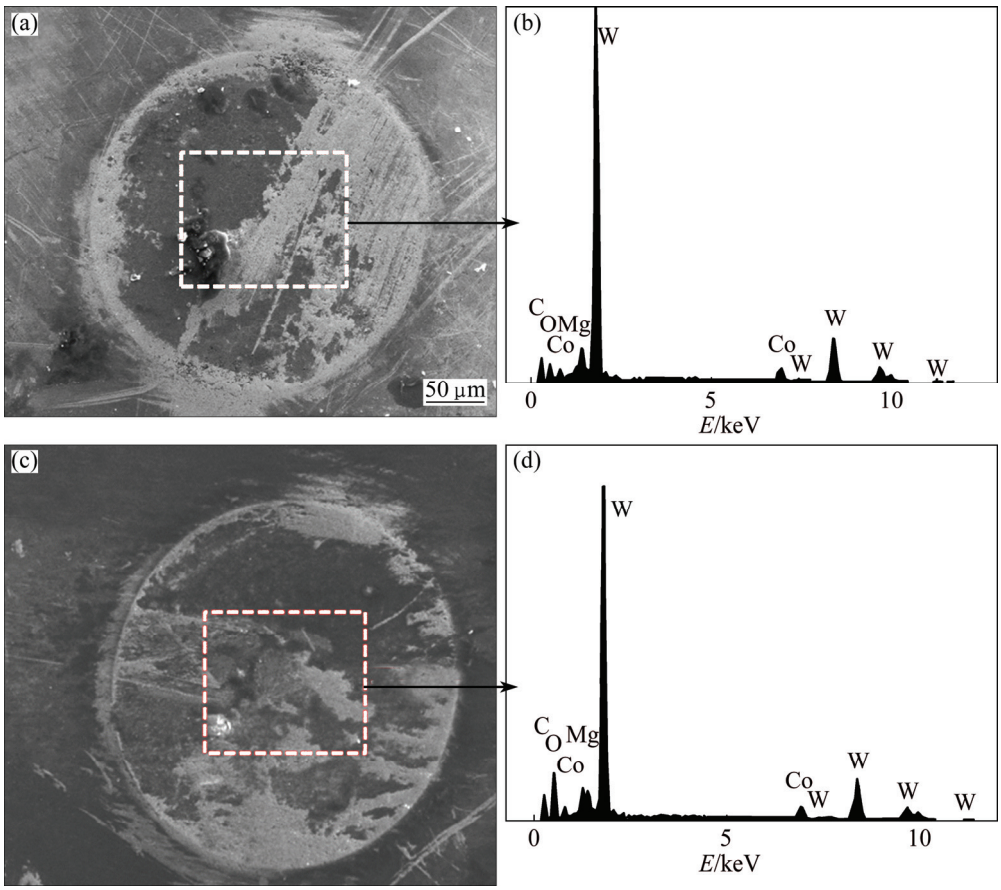


**Fig. 11** SEM images of wear scar on balls and corresponding EDS results: (a, b) Sliding against CrN coating; (c, d) Sliding against CrSiN coating

friction coefficient, better corrosion resistance and higher hardness.

4) The large flake pits exist on the wear track of CrN coating, indicating that the wear mechanism is dominated by local delamination and abrasive wear. However, the flake pits are eliminated by the addition of Si element, which is due to the finer crystal structure.

## References


[1] YANG Shu-dong, LI Zhuang-yun. Seawater hydraulic drive and its application in ocean exploitation [J]. Ocean Engineering, 18: 81−85. (in Chinese)

[2] SHAN Lei, WANG Yong-xin, LI Jin-long, LI He, WU Xue-dong, CHEN Jian-min. Tribological behaviours of PVD TiN and TiCN coatings in artificial seawater [J]. Surface and Coatings Technology, 2013, 226: 40−50.

[3] LIU C, BI Q, MATTHEWS A. EIS comparison on corrosion performance of PVD TiN and CrN coated mild steel in 0.5 N NaCl aqueous solution [J]. Corrosion Science, 2001, 43: 1953−1961.

[4] CUNHA L, ANDRITSCHKY M, PISCHOW K, WANG Z. Microstructure of CrN coatings produced by PVD techniques [J]. Thin Solid Films, 1999, 355: 465−471.

[5] OULD C, BADICHE X, MONTMITONNET P, GACHON Y. PVD coated mill rolls for cold rolling of stainless steel strips — Tribological and mechanical laboratory tests [J]. Journal of Manufacturing Processes, 2013, 15: 77−86.

[6] SHAN Lei, WANG Yong-xin, LI Jin-long, LI He, LU Xia, CHEN Jian-min. Structure and mechanical properties of thick Cr/$Cr_2N$/CrN multilayer coating deposited by multi-arc ion plating [J]. Transactions of Nonferrous Metals Society of China, 2015, 25(4): 1135−1143.

[7] SONG Gui-hong, LUO Zhuo, LI Feng, CHEN Li-jia, HE Chun-lin. Microstructure and indentation toughness of Cr/CrN multilayer coatings by arc ion plating [J]. Transactions of Nonferrous Metals Society of China, 2015, 25(3): 811−816.

[8] LU Li, WANG Qi-min, CHEN Bing-zhou, AO Yong-cui, YU Dong-hai, WANG Cheng-yong, WU Shang-hua, KIM Kwang-ho. Microstructure and cutting performance of CrTiAlN coating for high-speed dry milling [J]. Transactions of Nonferrous Metals Society of China, 2014, 24(6): 1800−1806.

[9] ALEGRÍA-ORTEGA J A, OCAMPO-CARMONA L M, SUÁREZ-BUSTAMANTE F A, OLAYA-FLÓREZ J J. Erosion–corrosion wear of Cr/CrN multi-layer coating deposited on AISI-304 stainless steel using the unbalanced magnetron (UBM) sputtering system [J]. Wear, 2012, 290−291: 149−153.

[10] RUDEN A, RESTREPO-PARRA E, PALADINES A U, SEQUEDA F. Corrosion resistance of CrN thin films produced by dc magnetron sputtering [J]. Applied Surface Science, 2013, 270: 150−156.

[11] ZHOU Fei, CHEN Kang-min, WANG Mei-ling, XU Xiao-jing, MENG Hua, YU Min, DAI Zhen-dong. Friction and wear properties of CrN coatings sliding against $Si_3N_4$ balls in water and air [J]. Wear, 2008, 265: 1029−1037.

[12] GENG Zhong-rong, WANG Hai-xin, WANG Cheng-bing, WANG Li-ping, ZHANG Guang-an. Effect of Si content on the tribological properties of CrSiN films in air and water environments [J]. Tribology International, 2014, 79: 140−150.

[13] AZZI M, BENKAHOUL M, SZPUNAR J A, KLEMBERG-SAPIEHA J E, MARTINU L. Tribological properties of CrSiN-coated 301 stainless steel under wet and dry conditions [J]. Wear, 2009, 267: 882−889.

[14] XU Xiang-min, ZHANG Hao, LUO Fei-fei, ZHOU Zi-hao, DUO Shu-wang. The properties of CrSiN coatings of different si content [J]. Applied Mechanics and Materials: Trans Tech Publ, 2014: 4323−4326.

[15] KIM G, KIM B, LEE S. High-speed wear behaviors of CrSiN coatings for the industrial applications of water hydraulics [J]. Surface and Coatings Technology, 2005, 200: 1814−1818.

[16] YOO Y H, HONG J H, KIM J G, LEE H Y, HAN J G. Effect of Si addition to CrN coatings on the corrosion resistance of CrN/stainless steel coating/substrate system in a deaerated 3.5 wt.% NaCl solution [J]. Surface and Coatings Technology, 2007, 201: 9518−9523.

[17] SANDU C S, SANJINÉS R, BENKAHOUL M, MEDJANI F, LÉVY F. Formation of composite ternary nitride thin films by magnetron sputtering co-deposition [J]. Surface and Coatings Technology, 2006, 201: 4083−4089.

[18] WANG Jun-jun, PU Ji-bin, ZHANG Guang-an, WANG Li-ping. Tailoring the structure and property of silicon-doped diamond-like carbon films by controlling the silicon content [J]. Surface and Coatings Technology, 2013, 235: 326−332.

[19] ZHANG Shi-hong, LI Ming-xi, HE Yi-zhu, CHO Tong-yul, CHUN Hui-gon, YOON Jae-hong, SI Song-hua, LI Hui-sheng. Synthesis and properties of $CrN_x$/amorphous-WC nanocomposites prepared using hybrid arc ion plating and direct current magnetron sputtering [J]. Thin Solid Films, 2010, 519: 751−758.

[20] WO P C, MUNROE P R, LI Z, JIANG Z T, XIE Z H, ZHOU Z F, LI K Y. Factors governing the mechanical behaviour of CrSiN coatings: Combined nanoindentation testing and transmission electron microscopy [J]. Materials Science and Engineering A, 2012, 534: 297−308.

[21] KONG Qing-hua, JI Li, LI Hong-xuan, LIU Xiao-hong, WANG Yong-jun, CHEN Jian-min, ZHOU Hui-di. Composition, microstructure, and properties of $CrN_x$ films deposited using medium frequency magnetron sputtering [J]. Applied Surface Science, 2011, 257: 2269−2274.

[22] LIPPITZ A, HÜBERT T H. XPS investigations of chromium nitride thin films [J]. Surface and Coatings Technology, 2005, 200: 250−253.

[23] LEE H Y, JUNG W S, HAN J G, SEO S M, KIM J H, BAE Y H. The synthesis of CrSiN film deposited using magnetron sputtering system [J]. Surface and Coatings Technology, 2005, 200: 1026−1030.

[24] WANG D Y, WENG K W. Microstructure analyses of CrN coating synthesized by a hybrid PVD and metal-plasma ion implantation process [J]. Surface and Coatings Technology, 2002, 156: 195−200.

[25] GELFI M, LA VECCHIA G M, LECIS N, TROGLIO S. Relationship between through-thickness residual stress of CrN-PVD coatings and fatigue nucleation sites [J]. Surface and Coatings Technology, 2005, 192: 263−268.

[26] BENKAHOUL M, ROBIN P, GUJRATHI S C, MARTINU L, KLEMBERG-SAPIEHA J E. Microstructure and mechanical properties of Cr−Si−N coatings prepared by pulsed reactive dual magnetron sputtering [J]. Surface and Coatings Technology, 2008, 202: 3975−3980.

[27] ROOS J R, CELIS J P, VANCOILLE E, VELTROP H, BOELENS S, JUNGBLUT F, EBBERINK J, HOMBERG H. Interrelationship between processing, coatingproperties and functional properties of steered arc physically vapour deposited (Ti, Al)N and (Ti, Nb)N coatings [J]. Thin Solid Films, 1990, 193: 547−556.

[28] ZHOU Fei, WANG Xiao-lei, ADACHI K, KATO K. Influence of normal load and sliding speed on the tribological property of amorphous carbon nitride coatings sliding against $Si_3N_4$ balls in water [J]. Surface and Coatings Technology, 2008, 202: 3519−3528.

[29] ALDRICH-SMITH G, TEER D, DEARNLEY P. Corrosion-wear response of sputtered CrN and S-phase coated austenitic stainless steel [J]. Surface and Coatings Technology, 1999, 116: 1161−1165.

# PVD CrN 和 CrSiN 涂层在海水环境中的腐蚀和磨损行为

单 磊[1,2,3]，章杨荣[1,2]，王永欣[1,2]，李金龙[1,2]，蒋 欣[1,2]，陈建敏[1,2]

1. 中国科学院宁波材料技术与工程研究所，中国科学院海洋新材料与应用技术重点实验室，宁波 315201；
2. 中国科学院宁波材料技术与工程研究所，浙江省海洋材料与防护技术重点实验室，宁波 315201；
3. 浙江纺织服装职业学院 机电分院，宁波 315211

**摘 要**：为提升 316L 不锈钢在海水中的耐磨性，采用多弧离子镀在 316L 不锈钢上沉积 CrN 和 CrSiN 涂层。对涂层进行系统地表征，用浸泡试验和极化测试评价涂层的耐腐蚀性能，用球−盘摩擦方式测试涂层在海水环境中的摩擦学性能。结果表明，CrN 涂层的衍射峰有很强的(111)和(200)取向，而 CrSiN 涂层的这两个峰相对较弱。CrSiN 涂层的硬度比 CrN 涂层略高，且 CrSiN 涂层表现出更优越的耐蚀性。CrSiN 在海水中的摩擦因数和磨损率相对 CrN 涂层均有所降低，表明掺杂元素 Si 有利于提高涂层在海水环境中的摩擦学性能。这两种涂层可有效提升 316L 不锈钢在海水中的耐磨性。

**关键词**：CrSiN 涂层；磨损；腐蚀；海水

**(Edited by Yun-bin HE)**